Korean J. Chem. Eng., 40(1), 223-234 (2023)
DOI: 10.1007/s11814-022-1283-0

pISSN: 0256-1115
eISSN: 1975-7220

Acid-doped polyaniline membranes for solar-driven interfacial evaporation

Xia Li[*,,***], Dongmin Yue[*,**], Fei Liu[*,**], Jingtong Yu[*,**], Bingbing Li[*,**,†], De Sun[*,**,†], and Xin Ma[***]**

*Department of Chemical Engineering, Changchun University of Technology, 2055 Yanan Street, Changchun 130012, P. R.China
**Key Laboratory of Advanced Functional Polymer Membrane Materials of Jilin Province, 2055 Yanan Street, Changchun 130012, P. R.China
***Department of Chemical Engineering, Benxi Chemical Industry School, 206 Fengye Road, Xihu District, Benxi, Liaoning Province, 110000, P. R. China

(*Received 30 April 2022 • Revised 11 August 2022 • Accepted 4 September 2022*)

Abstract−Interface solar desalination technology is an important green and sustainable strategy to solve the freshwater crisis. Herein, polyaniline (PANI) membranes were prepared by immersion precipitation phase inversion (NIPs) method and using for solar-driven water evaporation. To improve the light absorption rate of the PANI membrane, acid doping modification was carried out to the membrane. The results show that the polyaniline-p-toluene sulfonic acid (PANI-PTSA) membrane modified by p-toluene sulfonic acid (PTSA) has microporous structure, and the hydrophilicity was greatly improved after modification. The water evaporation rate and solar energy conversion efficiency of PANI-PTSA membrane were 1.38 kg/(m^2h) and 80.7% under 1 kW/m^2 sunlight irradiation, respectively, significantly improved compared to the original membrane. Due to the electrostatic repulsion effect of PANI-PTSA on anion charged SO_3^-, Na^+ is separated from Cl^-, which reduces the salt crystallization in the evaporator, indicating that PANI-PTSA membrane has certain salt resistance in solar desalination experiments. This work provides a simple method to prepare the PANI-PTSA membrane with high efficiency and salt resistance that has huge potential for practical application of interface solar desalination technology.

Keywords: Polyaniline, Photothermal Conversion, Interface Evaporation, Solar Desalination

INTRODUCTION

There is an urgent need for environmentally friendly and effective technologies and materials for sewage purification and seawater desalination with the increasingly serious global water pollution and decrease of water resources available for human direct use [1]. Seawater desalination is one of the most important ways to solve the shortage of water resources. Many countries have made seawater desalination a long-term development strategy for the consideration of human sustainable development [2,3].

Although there are many desalination methods, the energy consumption of making freshwater is still very high. At the same time, the pollutant emissions generated by burning fossil fuels by traditional desalination methods pose threats to the ecological environment [4]. Therefore, using green technology to produce drinking water has much potential. Solar-driven water evaporation (SWE), which combines the two most abundant resources on earth (solar and water), is considered one of the most attractive and easy to implement desalination technologies. With the assistance of photothermal materials, solar energy can be converted into heat energy for photothermal water evaporation, providing a green and promising way for water treatment. Solar desalination technology as a sustainable solution has aroused great interest in the scientific community.

The research on desalination, distillation and purification, sterilization and disinfection of seawater and brackish water by interfacial evaporation has become a new hotspot [7]. Solar-driven interfacial evaporation (SDIE) refers to the rapid evaporation process by using the micro-nano structure of materials to provide more liquid-gas contact interfaces [5]. Heat localization is concentrated at the gas-liquid interface based on the micro-nano structure, which realizes the efficient utilization of energy [6]. The SDIE device generates local heat at the evaporation interface, which avoids volume heating, reduces the heat loss of the bulk phase, and reduces the content of photothermal materials. As an effective method for low-cost desalination, this technology can realize the efficient utilization of low-grade solar energy, which will have great practical value.

The development of a membrane-based evaporation system has promoted the generation of high-efficiency solar evaporators, which can evaporate seawater even in the case of low solar intensity. These systems are usually used on the water surface. Because of their excellent solar light absorption capacity, they can effectively absorb solar energy and convert it into heat through plasma resonance on the metal surface and non-radiative transition of other materials. Under continuous lighting, the heat generated by the air-water interface instantly evaporates the water molecules around [8], resulting in continuous steam flow. This mechanism promotes more effective interface heating, which can effectively improve the overall evaporation performance of the system.

Photothermal materials are the most important and core com-

†To whom correspondence should be addressed.
E-mail: lbingbing2002@163.com, sunde@ccut.edu.cn

ponent of the photothermal evaporation system. Various photothermal membranes with excellent photothermal efficiency have been used for solar-driven evaporation. These membranes can be classified into carbon nanoparticles, organic materials, and metal plasma materials [9]. However, due to the high cost of raw materials and complex manufacturing process [10], large-scale application of these photothermal membranes has low economic benefits. With the development of near-infrared absorption technology, great progress has been made in the research and development of new near-infrared absorption materials. Among many photothermal conversion materials, organic conjugated polymers (such as polypyrrole, polyaniline, and polythiophene [11]) have become among the most promising photothermal materials. Compared with organic small molecular polymers, organic conjugated polymers show good light stability, high light absorption characteristics, low cost, low price and other advantages, which has become a hot polymer research topic. At the same time, polyaniline (PANI) has many advantages, such as diverse microstructure, special doping mechanism, stable combination with the substrate material and simple synthesis process, which make it an excellent solar interface evaporation photothermal conversion material [12]. PANI has three states: oxidation, reduction and intermediate. The structure of intermediate state of PANI obtained by doping is called emeraldimine salt. Because of its good near infrared absorption performance [13], it is an excellent photothermal material. PANI can cause electron transfer by doping to change the position of the absorption peak. When the imine group on PANI is transformed into imine salt, its near-infrared absorption is significantly enhanced. Bao et al. [14] synthesized a series of PANI with different HCl/aniline and DBSA/aniline molar ratio; the thermal stability for all PANI samples of different HCl/aniline molar ration was quite high. Guo et al. [15] synthesized polypyrrole (PPy) and polyaniline (PANI) nanoparticles which exhibited strong absorption in the near infrared (NIR) region with excellent photothermal efficiencies.

After acid doping of polyaniline, its near-infrared absorption can be significantly enhanced. In this paper, PANI photothermal conversion membranes were prepared by immersion precipitation phase inversion (NIPs), and then the photothermal properties of polyaniline were improved by doping different protonic acid. As shown in Fig. 1, the protonic acid connects the proton to the nitrogen atom of the PANI polymer chain through diffusion, which is the doping process. The membrane morphology, wettability, crystallization, chemical composition, pore size distribution, flux, rejection, optical absorption performance, interfacial evaporation and seawater desalination were studied. The acid-doped PANI photothermal conversion membrane with low cost, simple synthesis and long-term operation can be employed in the solar-driven interfacial evaporation.

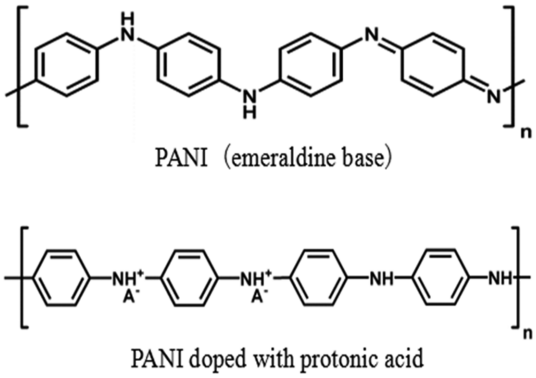

Fig. 1. The structure of eigenstate PANI and PANI doped with protonic acid.

EXPERIMENTAL

1. Materials

Polyaniline (molecular weight: 10,000-100,000, purity: ≥99.0 wt%, particle size: <30 μm) purchased from Cool Chemical Technology Beijing Co., Ltd; ammonium sulfate and ammonia were acquired from Aladdin Chemical Reagent Co., Ltd.; hydrochloric acid (HCl, 36 wt%-37 wt%). Acetic acid (HAc, 99.5 wt%) and p-Toluene sul-

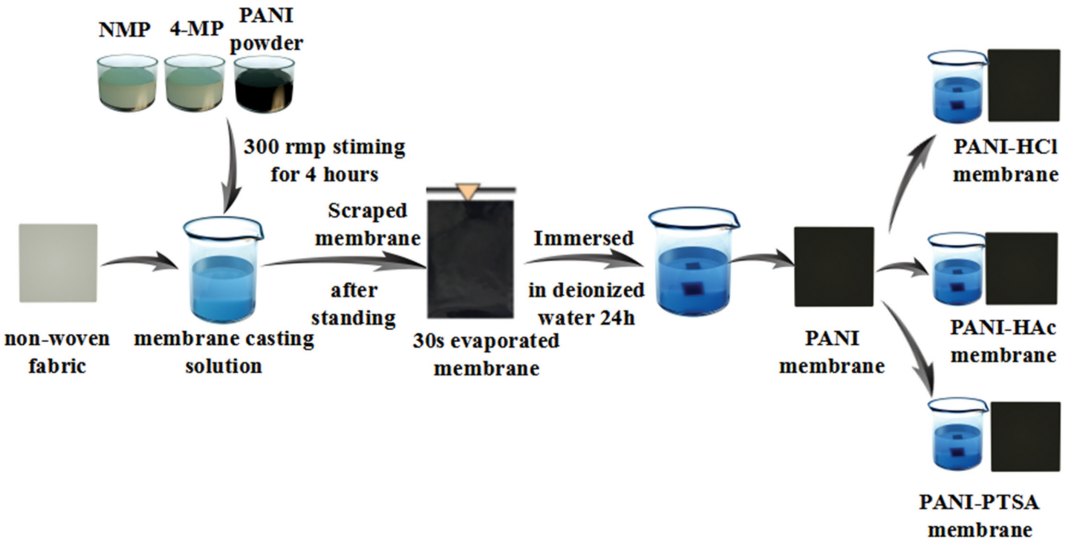

Fig. 2. Schematics of the fabrication procedure for PANI membrane.

fonic acid (PTSA, Molecular: 190.22) were purchased from Tianjin Fuyu Fine Chemical Industry Company; *N*-Methyl pyrrolidone *N*-Methyl pyrrolidone and 4-methylpiperidine were purchased from Shanghai McLean Biochemical Technology Co., Ltd. Nonwoven fabric was purchased from Haoxin insulation material Co., Ltd. Deionized water (Conductivity, 1 μs/cm) was self-produced in our laboratory.

2. Preparation of Acid-doped Polyaniline Membrane

The PANI membrane was prepared by NIPS method and the preparation process of acid-doped PANI membrane is shown in Fig. 3. The 4.00 g intrinsic polyaniline (PANI) powder was fully mixed with 15.42 g NMP and 2.65 g 4-MP. The mixture was stirred at about 350 rpm for 3 h to obtain a uniform PANI casting solution, and the non-woven fabric was fixed on the glass plate with transparent tape. Then the casting solution was cast on the nonwoven fabric at room temperature with a glass rod of 420 μm thickness. After evaporation for 30 seconds, the membrane was immersed in the coagulation bath of deionized water. The membrane was kept at room temperature for 24 hours, then washed with deionized water and stored in deionized water for standby. PANI membrane was cut into 3×3 cm square, and soaked in 1 mol/L hydrochloric acid, acetic acid, p-toluenesulfonic acid solution for 12 hours, respectively, named PANI-HCl membrane; PANI-HAc membrane; PANI-PTSA membrane.

3. Membrane Characterizations

The microscopic structure of membranes was characterized by scanning electron microscopy at 10 kV (SEM, JEOL JSM-7610, Japan). The roughness was tested and analyzed by the roughness profiler for membrane (Keyence VR-3200 G2 Japan). The infrared absorption spectra of PANI and its composite membranes were measured by Fourier transform infrared spectroscopy (FTIR) (Nicolet IS50 FT-IR, Thermofisher, USA). The infrared test wave number was set to be 4,000-525 cm^{-1}. The X-ray diffraction peaks of PANI and its composite membranes were detected by X-ray diffractometer (XRD, Rigaku/Smartlab) using K filtering method (45 kV, 200 mA). To determine the mechanical properties of PANI and its composite membranes, tensile tests were performed on a Universal testing machine (YHS-229WG, Shanghai Yihuan Company, China). The sample was cut into a rectangular strip of 50 mm× 10 mm and tested at a drawing speed of 2 mm min^{-1}. The thermal stability of PANI and its doped PANI photothermal composite membranes was tested by thermogravimetric analyzer. In the inert gas N_2 atmosphere, the gas flow rate was 50 mL/min, and the programmed temperature was set at a rate of 6 °C/min. The temperature was increased from 30 °C to 650 °C for detection. The water contact angles (WCA) of PANI and its composite membranes were measured by contact angle analyzer (HARKE-SPCA, Beijing) to evaluate the water wettability of the membrane. An appropriate amount of deionized water was pumped into the syringe. The optical absorption of PANI and its composite membranes was measured by UV-Vis-NIR spectrophotometer (Cary 5000, Agilent, USA) in the range of 300-2,500 nm by integrating sphere.

Conductivity of PANI and its composite membranes was measured by four-point probe technique using electrochemical workstation (PGSTAT302N, AUTOLAB). The membrane (1 cm×5 cm) was placed in the Teflon battery containing deionized water, and the battery had two current acquisition electrodes and two potential sensing electrodes (the distance between each two electrodes was 1.33 cm). Conductivity is calculated according to the following formula:

$$K = \frac{L}{PWd} \tag{1}$$

L (cm) is the distance between potential sensing electrodes, R (Ω) is the resistance of the membrane, W (cm) is the width of the membrane (1 cm), d (cm) is the thickness of the membrane.

The average pore diameter (r_m) of PANI and its doped PANI photothermal composite membrane was measured by capillary flow porosimeter (POROLUX 500, German). First, the sheared membrane was wetted with Profil liquid and placed in the sample chamber. Nitrogen at a flow rate of 0.05 MPa/min was used to flush up the lower surface of the membrane. The bubble point is the maximum pore size and the accumulated pressure is used to calculate the r_m and PSD.

Evaluation of average porosity (ε) of PANI and its composite membranes was by gravimetric method:

$$\varepsilon = \frac{w_1 - w_2}{(A \times l)\rho} \tag{2}$$

In this formula, w_1 is wet membrane mass (g), w_2 is dry membrane mass (g); a is the surface area (cm^2) of the membrane, ρ is the membrane thickness (cm), and ρ is the density of Profil liquid (1.87 g/cm^3 at 25 °C). An average value of more than three times was used as membrane porosity.

4. Solar-driven Interfacial Evaporation Performance

4-1. Photothermal Conversion and Interface Evaporation Experiments

To test the photothermal conversion performance of the membrane, an interface evaporation device was designed and fabricated, as shown in Fig. 4. The device is composed of three parts: solar simulator, evaporator and data acquisition. The solar simulator is provided by an Xe lamp (CEL-NP2000, Aulight Co., Ltd.) calibrated by an optical power meter with an AM1.5 filter (CHF-XM500, Beijing Trust Technology). The solar power meter (TES-132, TES Electrical Electronic Corp., China) is used to determine the optical density of the solar simulator, and the light intensity is maintained in one sun (1 kWm^{-2}). A 200 mL beaker was used as the container in the evaporator. The polystyrene foam coating cover was used as the thermal insulation device at the top of the beaker. A piece of 3 cm×3 cm polystyrene foam was cut in the middle and wrapped by cotton, and then put back to the original place. The cotton was penetrated into the deionized water of the beaker and used as the water channel through capillary action. The PANI membrane was placed on the cotton. The membrane surface temperature was measured by thermal imaging camera (E75, FLIR, USA). The data were collected by an electronic analytical balance with a precision of 0.0001 grams (JJ500Y, Changshu Shuangjie Electronic Balance Factory, China) to record the mass loss of solar steam generators.

Infrared thermal imaging camera (E75, FLIR, USA) was used to measure the temperature of interface between water and air and the temperature distribution of evaporator.

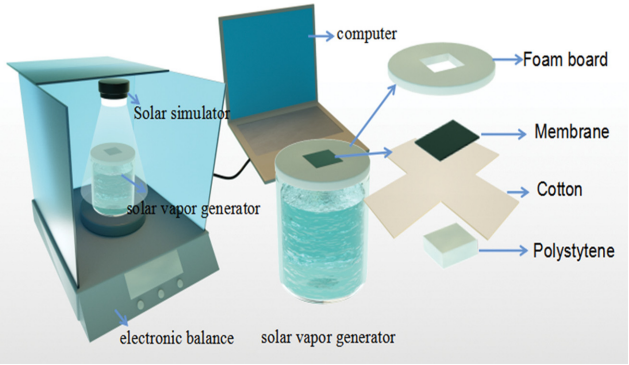

Fig. 3. Schematic diagram of interface evaporation device.

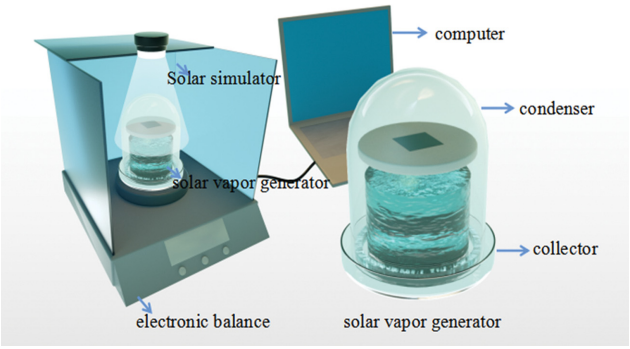

Fig. 4. Schematic drawing of desalination.

The whole water evaporation experiment was carried out at 25.0±0.5 °C, ambient temperature of 40±5% relative humidity, and the evaporation rate and energy conversion efficiency were calculated by mass loss after 2 h.

The steady state evaporation rate (m) and solar conversion efficiency (η) are calculated by the following formula:

$$\eta = \frac{m h_{LV}}{C_{opt} q_i} \tag{3}$$

where h_{LV} is the total enthalpy from liquid to gas phase, C_{opt} is the optical concentration, q_i corresponds to a solar energy (1 kW/m^2). m is the total evaporation rate minus the evaporation rate under dark conditions [16].

4-2. Seawater Desalination Experiment

To further test the salt deposition resistance of PANI membrane, 3.5 wt % NaCl solution was used to simulate seawater, and a seawater desalination experiment was carried out under simulated sunlight with light intensity of 1 sun for 13 h, as shown in Fig. 4. The evaporated steam was condensed by a condenser, collected and weighed by a glass dish, and the conductivity of the condensate was measured. The membrane surface of evaporation system was photographed before and after light to evaluate the salt accumulation.

NaCl rejection is calculated by the following formula:

$$R = 1 - \frac{c_p}{c_f} \tag{4}$$

The c_p and c_f are the NaCl concentrations in the permeate and feed, respectively.

RESULTS AND DISCUSSION

1. Morphology

Fig. 5 is SEM images of surface and cross section of PANI and acid doped PANI membranes. It can be seen that the upper surface of the PANI (emeraldine base) membrane is smooth. The dop-

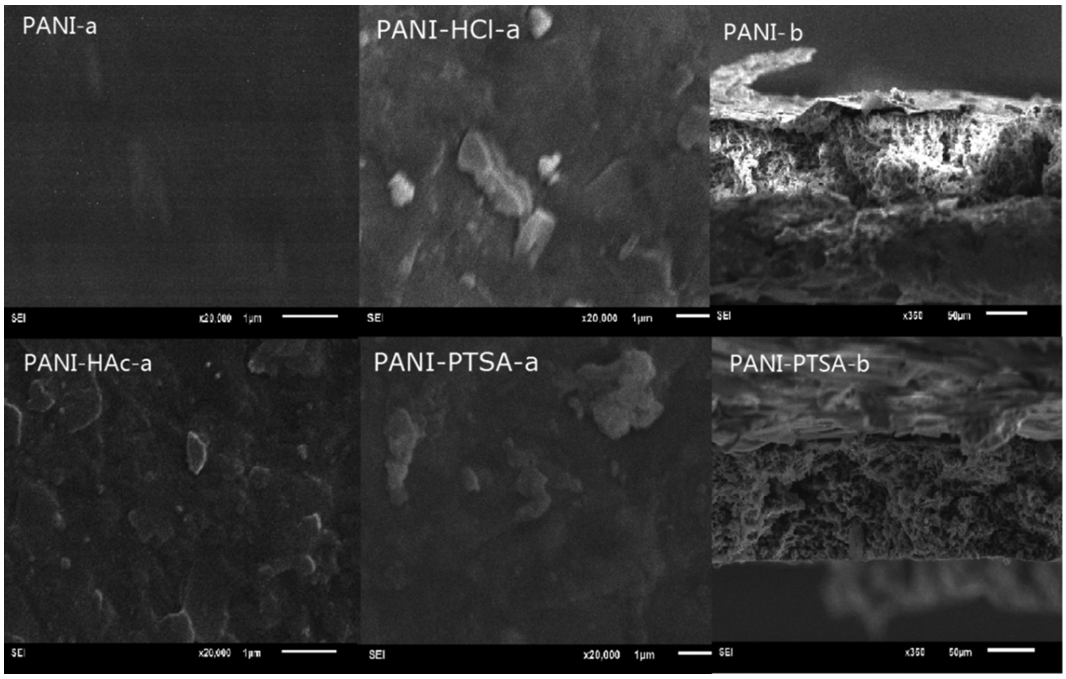

Fig. 5. SEM images, (a) magnification 20,000×; (b) (cross-section) magnification 350×.

Table 1. Surface roughness values of the membranes

Sa (mm)	Area 1	Area 2	Area 3	Area 4	Area 5	Area 6	Average
PANI	0.007	0.008	0.006	0.008	0.005	0.008	0.007
PANI-HCl	0.017	0.006	0.016	0.012	0.010	0.013	0.012
PANI-HAc	0.009	0.005	0.004	0.010	0.007	0.004	0.007
PANI-PTSA	0.004	0.005	0.007	0.005	0.005	0.003	0.005

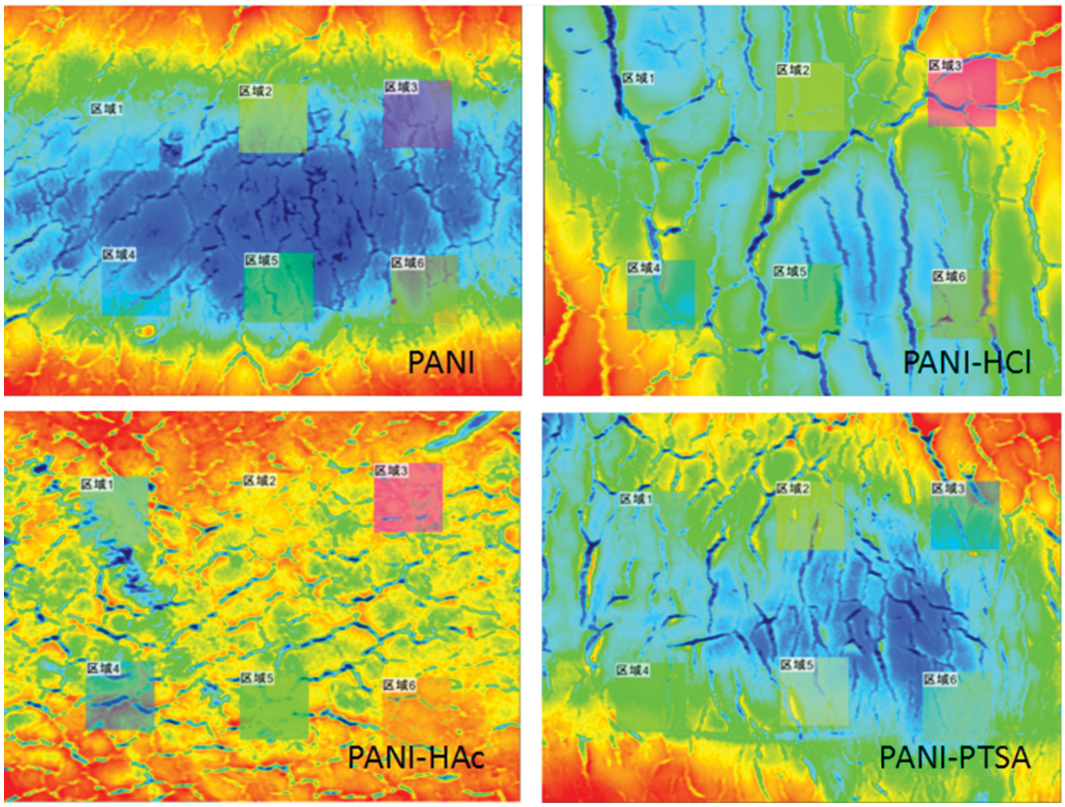

Fig. 6. Surface topography of the membranes.

ing of three kinds of acids has rough structure on the surface of the membranes. Among them, the HCl doped membrane presents uneven surface and block structure, because HCl is a strong acid. When the acidity is strong, it will cause excessive oxidation of PANI-HCl membrane and destroy its conjugate structure [17]. The roughness of PANI-HCl membrane is larger as shown in Table 1 and Fig. 6. Excessive oxidation may reduce the mechanical strength of the membrane, which is also consistent with the decrease in the mechanical strength of PANI-HCl membrane in the tensile strength test results of Fig. 9. HAc is a weak acid, and the oxidation degree of the membrane surface is significantly weaker than that of HCl. PTSA is an organic strong acid without oxidation, so the rough surface structures of PANI-HAc and PANI-PTSA are not obvious than that of PANI-HCl membrane. This is also consistent with the results of smaller roughness of PANI-HAc and PANI-PTSA membrane in Table 1 and Fig. 6.

Acid doping is a process in which protons enter the nitrogen atom of polyaniline quinone ring and reduce the quinone ring to benzene ring, resulting in the spatial reconstruction of the polymer [18]. The arrangement of the polymer is more orderly, which may be due to the fact that the molecular chains of PANI are embedded in the opposite anions of macromolecule size [19], weakening the interaction between the chains and reducing the agglomeration of the polymer. From the cross section diagram, it can be seen that both PANI and PANI-PTSA membranes have sponge-like structure, and that of PANI-PTSA are more orderly than the PANI membrane, which is also consistent with the doped polyaniline in the literature [20].

2. FTIR

The surface chemical composition of PANI membranes tested by infrared spectra. Fig. 7 shows the infrared spectra of PANI membrane and doped PANI membranes. The functional group structure represented by the absorption peak of PANI is as follows: 1,551 cm^{-1} corresponds to the quinoid ring, 1,475 cm^{-1} corresponds to the benzene ring, 800 cm^{-1} is the out-of-plane bending vibration peak of C-H in the benzene ring [21], and 1,238 cm^{-1} is the stretching vibration peak of C-C double bond on the quinoid ring. The functional group structure represented by the absorption peak

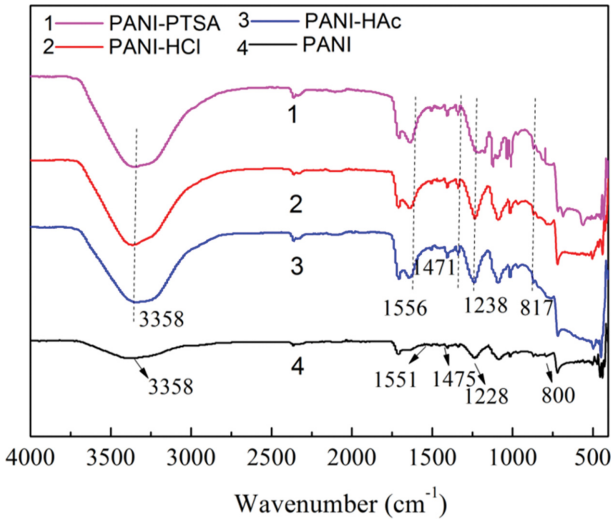

Fig. 7. FTIR spectra, 1: PANI-PTSA; 2: PANI-HCl; 3: PANI-HAc; 4: PANI.

of acid doped polyaniline is as follows: 1,556 cm^{-1} corresponds to quinone ring, 1,471 cm^{-1} is benzene ring, the characteristic absorption peak position of acid doped polyaniline quinone ring moves 5 cm^{-1} to the high wave number direction, the characteristic absorption peak position of benzene ring changes little, the stretching vibration peak of carbon-carbon double bond on quinone ring moves 10 cm^{-1} to the high wave number direction, the vibration peak of 797 cm^{-1} is C-H out-of-plane bending vibration in benzene ring. This indicates that doping mainly occurs on the nitrogen atom of the quinoid ring, rather than on the nitrogen atom of the benzene ring [22,23]. At the same time, the -OH peak at 3,358 cm^{-1} is hydroxy peak of water due to the increase of hydrophilicity caused by acid doping.

3. XRD

The crystallinity of PANI membranes was characterize by XRD.

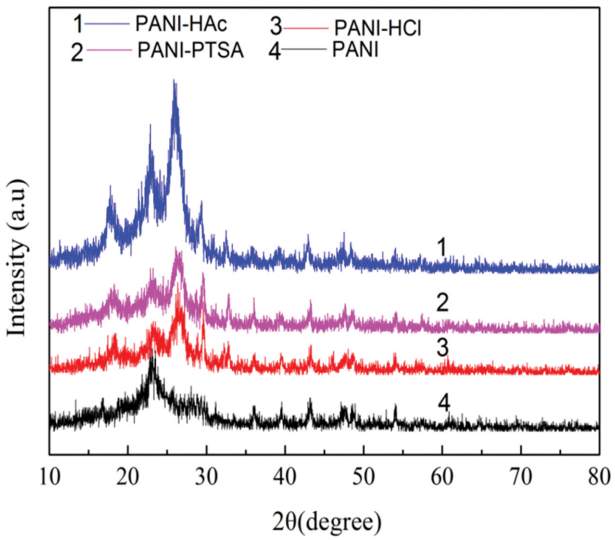

Fig. 8. XRD spectra, 1: PANI-HAc; 2: PANI-PTSA; 3: PANI-HCl; 4: PANI.

Fig. 8 is the XRD patterns of PANI membranes and acid-doped PANI membranes. The intrinsic polyaniline only has a very wide diffraction peak at 20° [24], which is the characteristic peak of amorphous polyaniline. It is attributed to the diffraction of the molecular chain of the intrinsic polyaniline, indicating that the intrinsic polyaniline is in a typical amorphous state with short-range order and weak orientation. The crystalline peaks of doped PANI at 18.0°, 20.0° and 25.2° can be the (011), (020) and (200) crystal planes of doped PANI [25]. The characteristic peaks at 18.0° and 25.2° are attributed to the periodicity perpendicular to and parallel to the polymer chain [26]. The peak at 20.0° is caused by the alternation of polymer chains [27]. The diffraction peaks of doped polyaniline at 20.0° and 25.2° are sharper, indicating that the orientation of PANI doped with protonic acid is orderly and the crystallinity is improved. This is due to protonic acid doping induced protonation of cations into the molecular chain part of the N atom and the subsequent entry of ions forming a similar "quaternary ammonium salt" structure [28], strengthening the interaction between molecular chains [29].

4. Membrane Conductivity

Fig. 9 is the conductivity of PANI membrane and acid doped PANI membrane after wetting with deionized water. It was found that the conductivity of PANI membrane increased from 0.12 S/cm to 0.43 S/cm after acid doping. H^+ generated by acid decomposition and protonation reaction into the main chain [30], the anion will also enter the PANI molecular chain to maintain the electrical neutrality. In the process of protonic acid doping, the number of electrons in the PANI chain did not change, and the N atoms in the amine and imine groups combined to form polarons and bipolarons and delocalized into the P bond of the whole molecular chain [21], so that polyaniline showed high conductivity. The PANI chains with secondary doping strong acid properties were connected in the form of head and tail [31], and the conductivity was relatively high. The PANI chains doped with weak acidic protonic acid are connected in a header manner, and the conductivity is relatively low. PTSA is a strong organic acid and the larger the anion is, the easier it is to be doped in PANI molecules, because

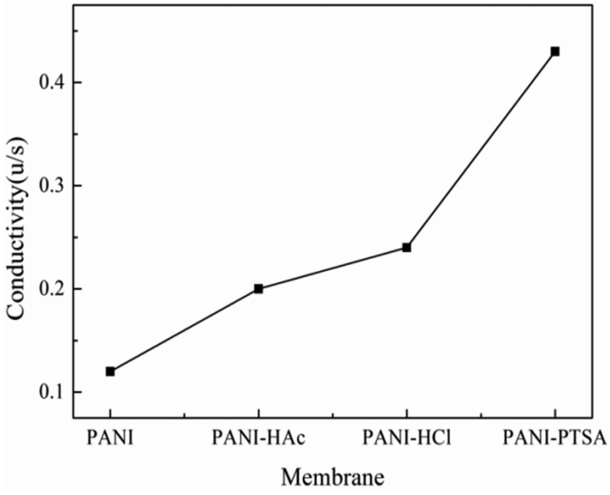

Fig. 9. Conductivity of PANI and PANI doped with acid membranes.

Table 2. Pore sizes and Porosity of the PANI and PANI doped with acid membranes

Membrane \ Pore size	Maximum (μm)	Mean (μm)	Minimum (μm)	Porosity (%)
PANI	4.49	1.50	0.37	52.74
PANI-HCl	1.66	1.47	1.07	43.76
PANI-HAc	3.33	1.38	0.56	50.13
PANI-PTSA	2.49	2.30	2.00	50.99

large anions can reduce the interaction between PANI molecules, which is conducive to charge delocalization and improve its conductivity [17]. Since the conductivity of polyaniline reflects the doping degree of doped acid to a certain extent [32], the test results prove that protonic acid is successfully doped and may reconstruct the polymer structure.

5. Average Pore Size and Porosity of Membrane

The pore structure of photothermal membranes is crucial for light absorption capacity and water transport capacity. Table 2 and Fig. 10 show pore size and pore size distribution (PSD) of PANI and acid doped PANI membranes. After adding acid, the pore size range becomes narrow and the maximum pore size decreases obviously. The maximum pore size of PANI-HCl is 1.66 μm, which is close to the minimum pore size of 1.07 μm. Therefore, acid doping makes the pore size of PANI membrane tend to be uniform, which may be caused by the stress change caused by acid doping. Especially, the acid effect is obvious at the macropores, resulting in the interphase force of PANI and reducing the macropores. However, this interphase force blocked some small pores. It can also be seen from the table that the minimum pore size increased, so the porosity decreased slightly after adding acid.

6. Mechanical Properties of Membranes

Fig. 11 shows the tensile strength and elongation at break of PANI membrane and acid doped PANI membranes. With the doping of acid, the tensile strength and elongation at break decreased slightly. According to Reference [18], the acid doping agent of PANI would affect the intermolecular reconstruction of the main chain. As shown in Fig. 8 XRD, the proton acid doped PANI has ordered orientation, high crystallinity and increased mechanical strength. but a stress effect was generated between different crystalline phases [33]. Therefore, the acid doping would reduce the membrane strength. On the other hand, for acid doped PANI membranes, the decrease of porosity and macropores can also improve the mechanical strength of acid doped PANI membranes [11] in Table 2.

7. TGA

Fig. 12 is the thermodynamic properties of PANI membrane and acid doped PANI membrane. The weight loss of intrinsic PANI before 120 °C is due to the volatilization of residual water [34], which is similar to that of various acid-doped membranes. The weight loss between 130 °C and 240 °C is due to the removal of dopants from the material. The removal temperatures of hydrochloric acid (HCl) and acetic acid (HAc) are low, so HCl and HAc are easy to escape at high temperatures and dedoped [35]. Methylbenzenesulfonic acid (PTSA) and PANI have similar decomposition tempera-

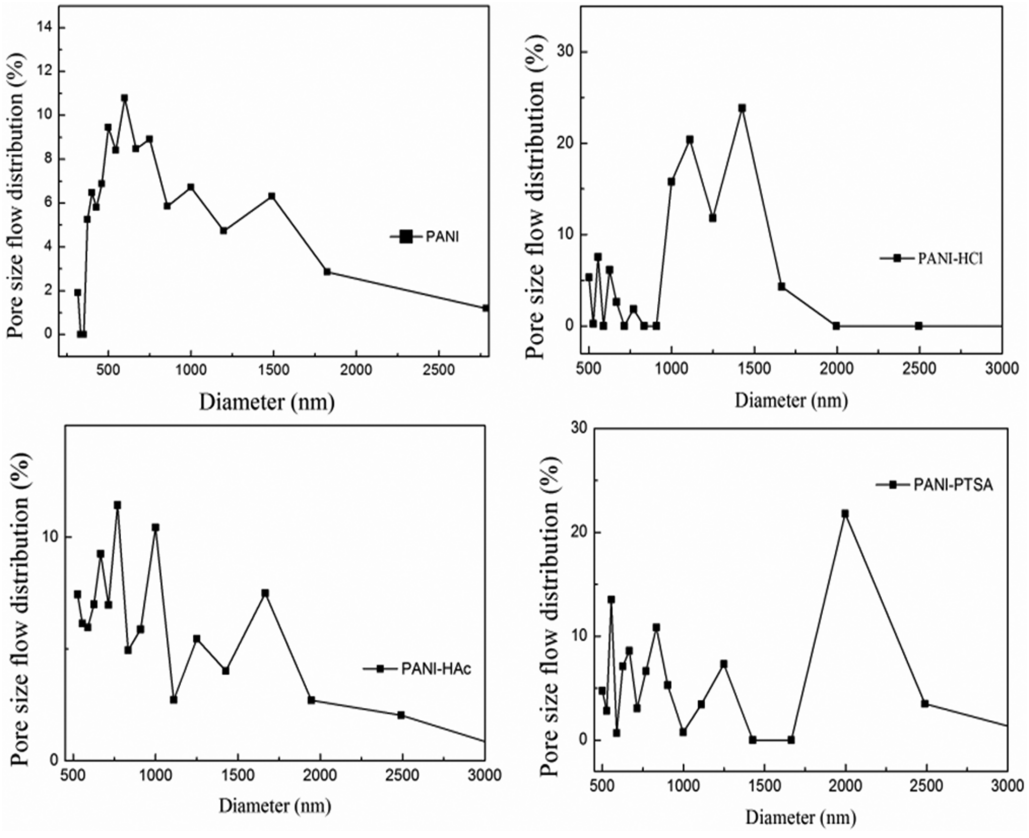

Fig. 10. Pore size distribution of membranes.

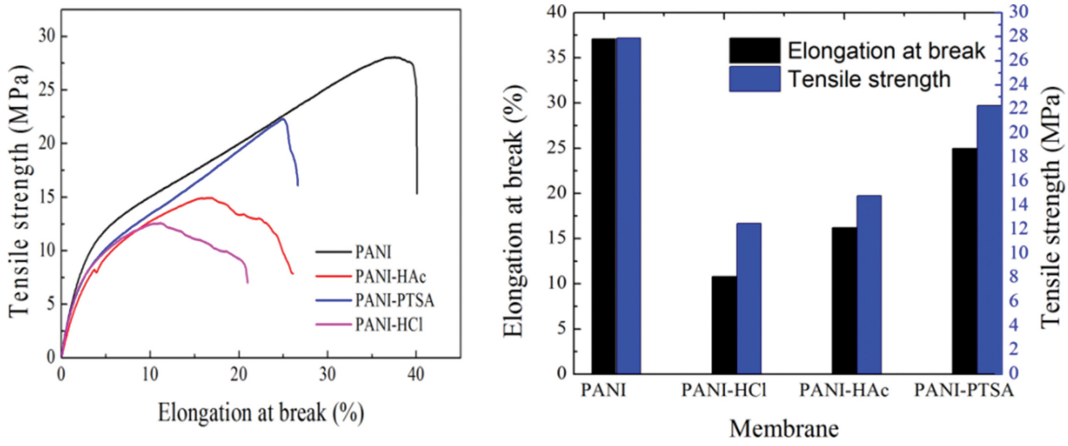

Fig. 11. Tensile strength (MPa) and elongation at break (%).

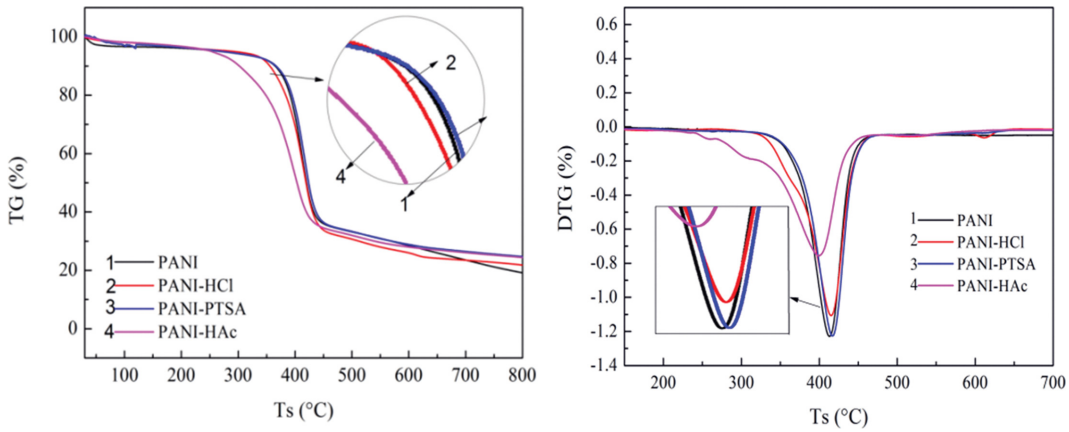

Fig. 12. Thermogravimetric analysis: 1: PANI; 2: PANI-HCl; 3: PANI-PTSA; 4: PANI-HAc.

ture. The weight loss above 450 °C is caused by the degradation of macromolecular chains [34]. PANI is similar to each doped acid membrane, and PANI is completely decomposed above 650 °C. Considering the practicality of materials and the need for photothermal experiments under continuous light conditions, hydrochloric acid (HCl) and acetic acid (HAc) are easy to volatilize, and dedoping is not conducive to the long-term stability of the experiment. The decomposition temperature of p-toluenesulfonic acid (PTSA) is higher than that of acetic acid (HAc) and hydrochloric acid (HCl). The reason may be that organic acids are not easy to volatilize, and large volume anions enhance the interaction between molecular chains, hindering the degradation between molecular chains, and are not easy to dedope, so they are more conducive to the long-term stability of interfacial evaporation [36].

8. Hydrophilicity of Membrane

Fig. 13 shows the water contact angle on the membrane surface. The results show that the water contact angle of the PANI membrane doped with acid decreased from 69.5° of the original membrane to the minimum of 46.9°. Since sulfonic acid group and carboxylic acid group are hydrophilic, polar solvent hydrochloric acid makes PANI produce ammonium salt structure, which improves the hydrophilicity of doped membrane. Compared with the water contact angle of PANI membrane at 69.0°, PANI-HAc membrane

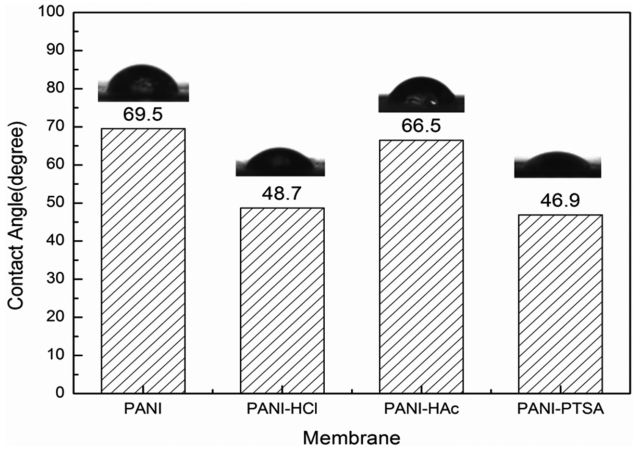

Fig. 13. Water contact angles of the PANI membrane and PANI doped with acid membrane.

and PANI-PTSA membrane have better hydrophilicity, and superior hydrophilicity can ensure the water supply of interfacial evaporation [37].

9. Optical Absorption Performance

The light absorption rates of PANI, PANI-HCl, PANI-HAc and

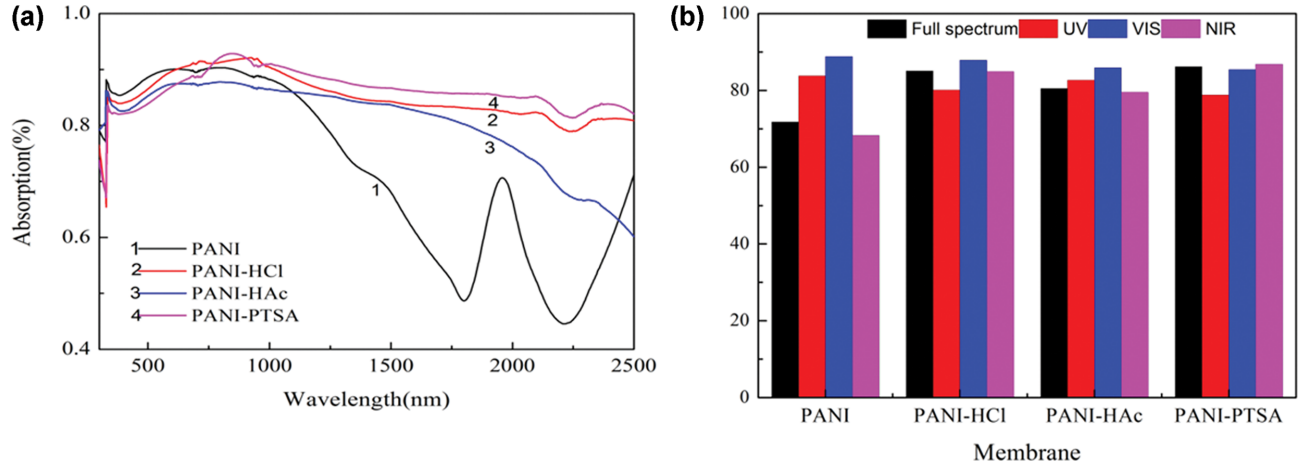

Fig. 14. (a) UV-vis-NIR spectra of the membranes, (b) Absorption rates of the membranes in each band.

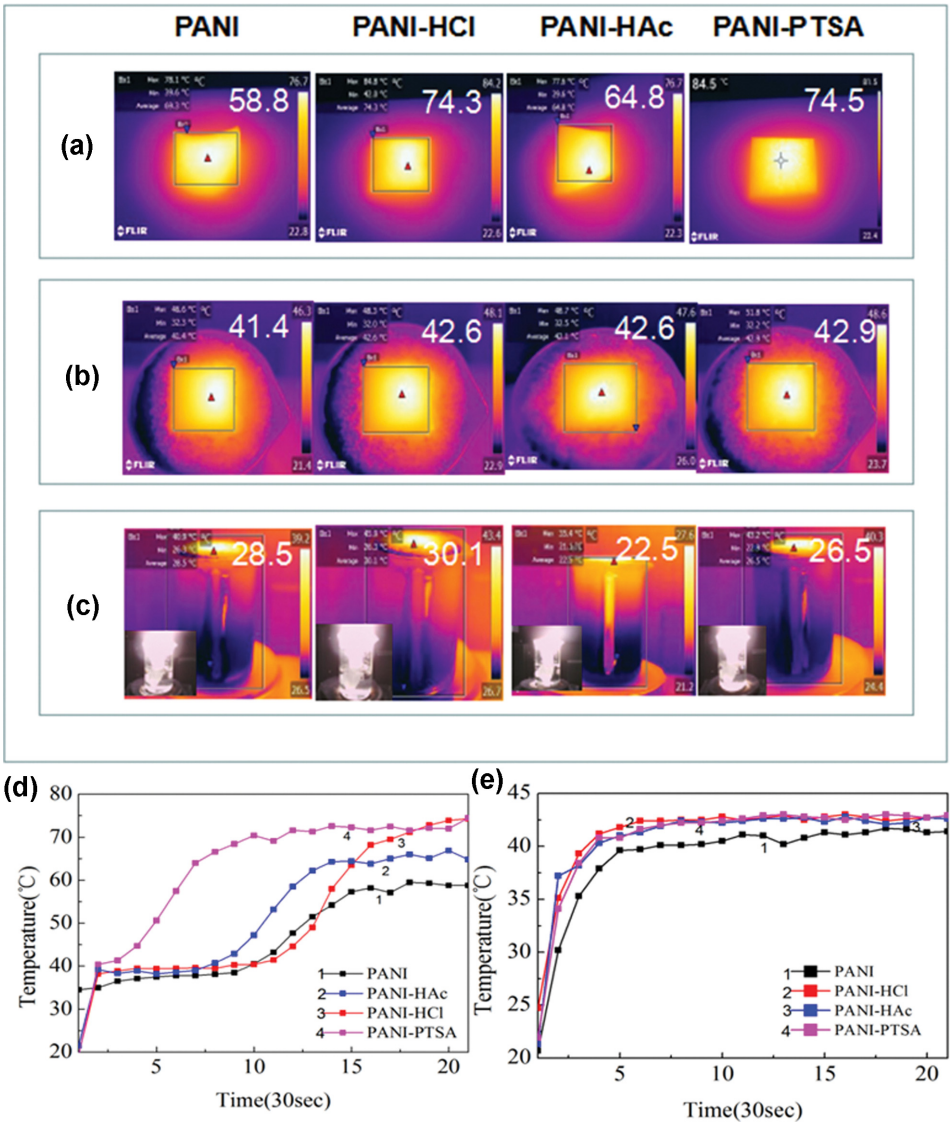

Fig. 15. (a) Temperature distribution of dry membranes in air under 1 sun; (b) Temperature distribution of wet membranes on the evaporator under 1 sun; (c) Temperature distribution of the membranes in evaporator under 1 sun; (d) Temperature change of dry membranes in air under 1 sun; (e) Temperature change of wet membranes in evaporator under 1 sun.

PANI-PTSA in the whole solar spectral range were measured by UV-Vis-NIR spectrophotometer, as shown in Fig. 14(a). In the solar spectrum, the ultraviolet region accounts for about 3% of the total energy, the visible region accounts for about 45% of the total energy, and the near-infrared region accounts for about 52% of the total energy. The absorption rates of ultraviolet (300-400 nm), visible (400-700 nm), near-infrared (700-2,500 nm) regions and the whole solar spectrum of the photothermal membrane was calculated in proportion, as shown in Fig. 14(b). By comparison, the infrared absorption of PANI-PTSAmembrane (86.8%) was significantly improved, which was 18.5% higher than that of the original PANI membrane (68.3%), and the average absorption rate of the whole solar spectrum was increased by 14.4%. This is due to the red shift of the UV absorption peak of doped polyaniline and the increase of the conjugated degree of polyaniline molecules, which makes the polyaniline chain interact with the benzene ring on the p-toluenesulfonic acid, and the electronic activity range on the delocalized π bond becomes larger. PANI-PTSA membrane shows strong broadband solar light absorption, which is beneficial to the demand for photothermal conversion.

10. Photothermal Experiments

10-1. Photothermal Conversion Experiments

Fig. 15 shows photothermal conversion performance of PANI membrane, doped PANI membrane. It can be found that the temperature of the membrane in the air is obviously higher than that in the evaporator, which is caused by the evaporation and heat absorption of water. At the same time, the temperature of PANI membrane doped with acid is significantly higher than that of the original PANI membrane, which shows that doping protonic acid can improve the photothermal conversion of PANI membrane, and the photothermal conversion effect of PANI-PTSA membrane is the best. In Fig. 15(c), evaporator surface photothermal conversion membrane temperature is significantly higher than the evaporator internal liquid temperature, which shows that the photothermal conversion membrane can play a role in local heating, can effectively improve the utilization of solar energy. Fig. 15(d) and (e): the temperature of all membranes shows a trend of rising first and then maintaining equilibrium. The temperature of PANI membrane doped

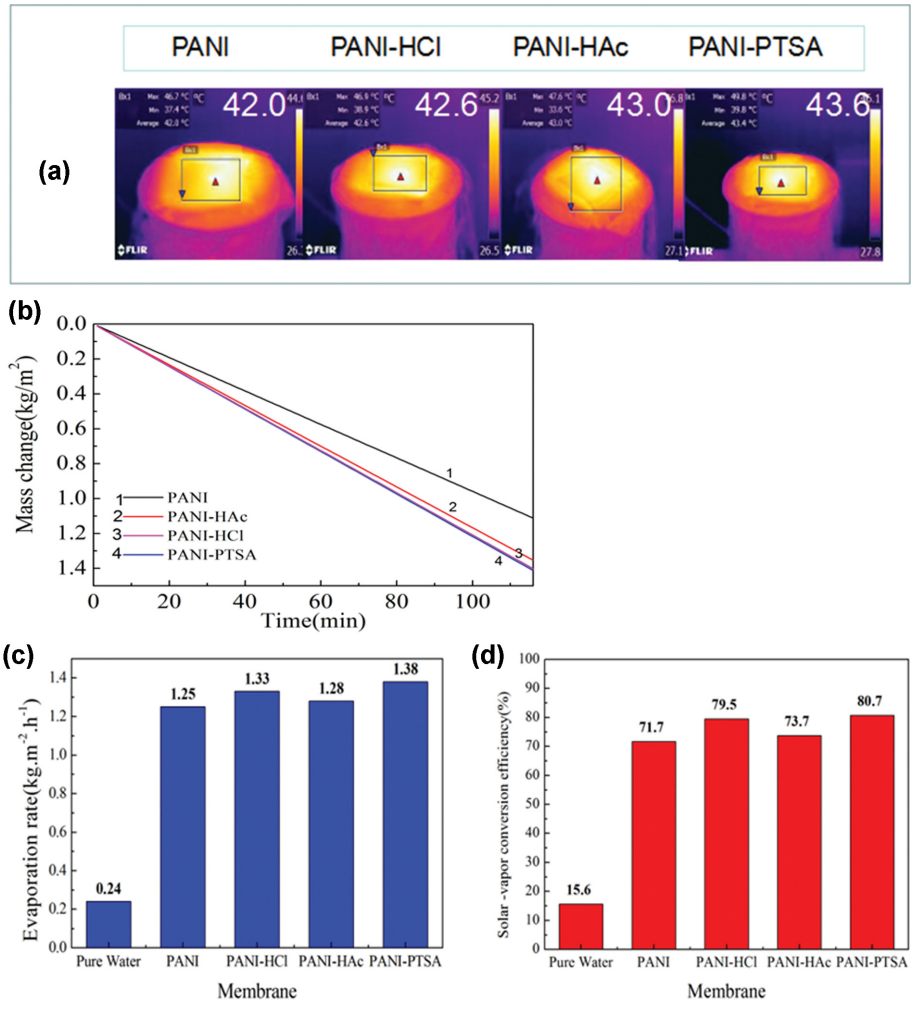

Fig. 16. (a) Temperature distribution of PANI membrane and PANI doped with acid membrane on the evaperator under 1 sun 2 h later; (b) Mass change of PANI membrane and PANI doped with acid membrane under 1 sun. (c) The evaporation rate of the PANI membrane and PANI doped with acid membrane under 1 sun. (d) The solar-vapor conversion effective of PANI membrane and PANI doped with acid membrane.

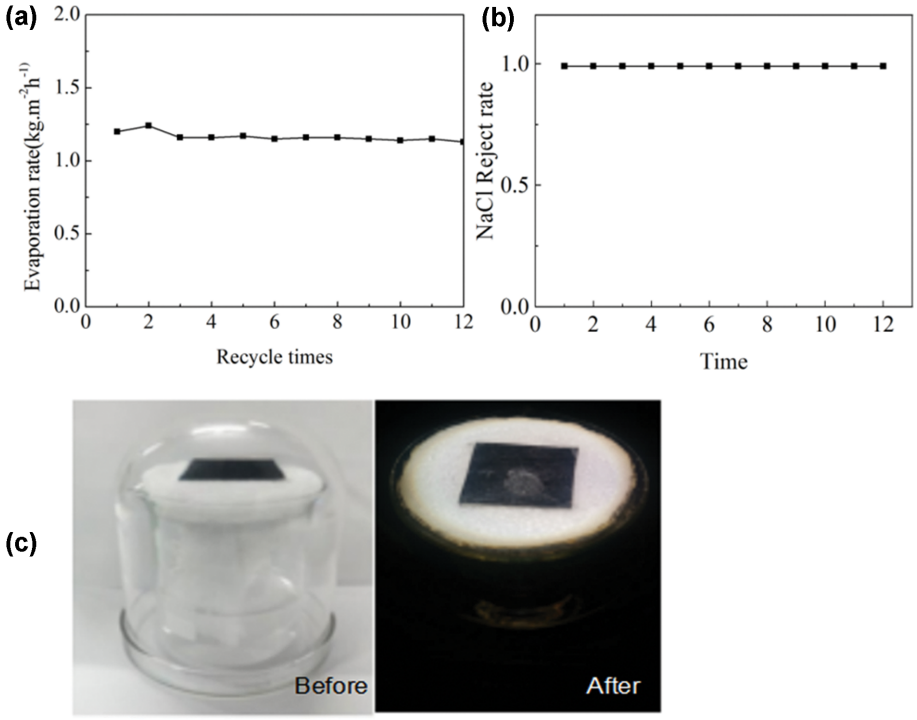

Fig. 17. (a) Long-term performance of PANI doped with acid membrane (feed: 3.5 wt% NaCl solution). (b) salt resistance rate of PANI membrane and PANI doped with acid membrane. (c) Photograph of the salt resistance of PANI doped with acid membrane (feed: 3.5 wt% NaCl, under 1 sun, 13 h).

by acid was significantly higher than that of PANI original membrane, and the temperature of PANI-PTSA membrane was the highest. This is due to the doping of protonic acid to improve the near infrared light absorption rate, which is consistent with the experimental results of 3.9 light absorption performance.

10-2. Interface Evaporation Experiment

Fig. 16 shows the interfacial evaporation properties of PANI and acid-doped PANI photothermal conversion membranes. It can be seen from Fig. 16(a) that the average temperature of the membrane surface was stable at 42 °C-43 °C after 2 h of operation, and the temperature of the membrane surface after acid doping was significantly higher than that of PANI membrane. From Fig. 16(b), the weight loss after acid doping was significantly higher than that of PANI membrane, and the weight loss of PANI-PTSA membrane was the fastest and most, indicating that high photothermal conversion performance was conducive to improving the interfacial evaporation performance of the membrane. From Fig. 16(c), compared with the pure water ratio without the photothermal conversion membrane, the photothermal conversion membrane can effectively improve the water vapor evaporation rate of the membrane. At the same time, the effect of the acid-doped PANI membrane is significantly higher than that of the original PANI membrane (1.25 kg/(m^2h)), which is caused by the improvement of the near-infrared light absorption rate by proton acid doping. The water vapor evaporation rate of PANI-PTSA membrane is the highest, which can reach 1.38 kg/(m^2h), which is 5.75 times and 1.1 times that of pure water and original membrane, respectively. Fig. 16(d) shows the evaporation rate of 0.10 kg/(m^2h) of water vapor evaporation under the condition of removing darkness. The evaporation efficiency of photothermal conversion membrane is significantly higher than that of pure water, and the evaporation efficiency of PANI-PTSA membrane is the highest, which can reach 80.7%.

10-3. Solar Desalination Performance

Based on the excellent solar thermal properties of PANI-PTSA membrane, it is applied to solar desalination. The PANI-PTSA membrane was placed on the evaporator surface with simulated seawater (3.5 wt% NaCl solution) and desalted under 1 sun light. The water vapor evaporation rate of the PANI-PTSA membrane is shown in Fig. 17(a). After 13 cycles, the water vapor evaporation rate of the PANI-PTSA membrane was still maintained at about 1.16 kg/(m^2h) without significant decrease, which verifies the cyclic stability of the PANI-PTSA membrane. At the same time, the goal of seawater desalination is to separate sea salt from seawater to obtain fresh water. To quantitatively study the purification performance of acid-doped PANI membrane, the rejection rate of NaCl was calculated by measuring the conductivity of condensed water. After 13 cycles of PANI-PTSA membrane, the rejection rate of NaCl could reach 99.99%, and the concentration was far below the drinking water standard stipulated by the World Health Organization (WHO). Fig. 15(c) is the contrast figure before and after 13 desalination cycles. It can be found that the evaporation surface of PANI-PTSA membrane has slight salt crystallization. This is because PTSA effectively separates Na^+ from Cl^- through electrostatic repulsion effect on anionic negatively charged SO_3, thereby reducing the formation of salt crystals on the evaporator. The PANI-PTSA membrane achieved certain salt resistance and long-term evaporation

stability under sunlight. These results show that PANI-PTSA membrane can maintain a long-term stable evaporation rate in the solar simulator.

After continuous illumination for 13 h under 1 sun, the condensed water was collected (Fig. 17(c)), and the daily water yield of PANI-PTSA membrane was calculated to be 15.08 L/m^2. These results show that PANI-PTSA membrane has good seawater purification ability.

CONCLUSION

Doped PANI membrane, PANI-HCl membrane, PANI-HAc membrane and PANI-PTSA membrane were prepared by proton acid doping method and used for solar seawater desalination. The photothermal conversion performance of the membrane was studied. The main conclusions are as follows:

(1) Superior hydrophilicity provides favorable conditions for interfacial evaporation.

(2) The solar spectral absorption of the proton acid doped p-toluene sulfonic acid (PANI-PTSA) membrane was significantly improved compared with that of the original membrane (PANI). The infrared absorption increased by 18.5%, and the average absorption rate of the whole solar spectral absorption increased by 14.4%.

(3) The PANI-PTSA membrane has an efficient and stable evaporation rate and evaporation efficiency, with the evaporation rate of 1.38 kg/(m^{2}h) and the solar energy conversion efficiency of 80.7%.

(4) Solar desalination experiment has long-term stability. After 13 cycles at 1 sun, the evaporation rate of PANI-PTSA membrane can be maintained at about 1.16 kg/(m^{2}h), and the water evaporation rate and solar conversion efficiency of PANI-PTSA membrane are relatively stable within 13 h. The electrostatic repulsion effect of PTSA on anionic negatively charged SO_3^- makes Na^+ and Cl^- separate, reducing the salt crystallization on the evaporator. The studies also show that PANI-PTSA membrane has certain salt resistance in solar desalination experiments.

ACKNOWLEDGEMENTS

Authors acknowledge the financial support from National Key R&D Plan under grant 2018YFB0504600, 2018YFB0504603. The Natural Science Foundation of Jilin Province (grant number 20210101392JC).

REFERENCES

1. Y. Yang and Z. Shao, *Nanotechnology*, **33**, 185403 (2022).
2. A. D. Khawaji and J. M. Wie, *Desalination*, **98**, 135 (1994).
3. D. Lin, Y. Liu, Z. Liang, H. W. Lee, J. Sun, H. Wang, K. Yan, J. Xie and Y. Cui, *Nat. Nanotechnol.*, **11**, 626 (2016).
4. X. Xuan, B. Xu, D. Sinton and D. Li, *Lab on A Chip*, **4**, 230 (2004).
5. C. Wang, L. Wang, W. Liang, F. Liu and A. Li, *J. Colloid Interface Sci.*, **605**, 60 (2021).
6. J. Cao, W. Fu, H. Yang, Q. Yu, Y. Zhang, S. Wang, H. Zhao, Y. Sui, X. Zhou, W. Zhao, Y. Leng, H. Zhao, H. Chen and X. Qi, *Mater. Sci. Eng. B*, **175**, 56 (2010).
7. E. Ye, A. Jl, B. Hl, A. Eyl, Y. Dong, A. Ysj, A. Jhh and H. Sang, *Chemosphere*, **291**, 133013 (2022).
8. X. Miao, S. Liu, M. Wang, B. Ge and C. Q. Zhu, *Sci. China Technological Sci.*, **64**, 2292 (2021).
9. A. Lalisse, G. Tessier, J. Plain and G. Baffou, *Sci. Rep.*, **6**, 38647 (2016).
10. M. Elimelech and W. A. Phillip, *Science*, **333**, 712 (2011).
11. Z. Song, W. Zhi, J. Wang, S. Yang and S. Wang, *J. Membr. Sci.*, **376**, 83 (2011).
12. L. Wang and B. Geng, *Appl. Mech. Mater.*, **633-634**, 302 (2014).
13. Z. Zhang, G. H. Wang, W. Gu, Y. Zhao and G. Ji, *J. Colloid Interface Sci.*, **605**, 193 (2022).
14. L. Bao and X. Liu, *IOP Conf. Ser. Mater. Sci. Eng.*, **772**, 012048 (2020).
15. B. Guo, J. Zhao, C. Wu, Y. Zheng, C. Ye, M. Huang and S. Wang, *Colloids Surf. B: Biointerfaces*, **177**, 346 (2019).
16. L. Sun, J. Liu, Y. Zhao, J. Xu and Y. Li, *Carbon*, **145**, 352 (2019).
17. S. Yu and J. Shi, *Contemp. Chem. Ind.*, **40**, 66 (2011).
18. L. Xu, S. Shahid, A. K. Holda, E. Emanuelsson and D. A. Patterson, *J. Membr. Sci.*, **552**, 153 (2018).
19. H. F. Alesary, H. K. Ismail, M. Q. Mohammed, H. N. Mohammed, Z. K. Abbas and S. Barton, *Chem. Papers*, **75**, 5087 (2021).
20. J. J. Li, X. F. Tang, H. Li, Y. G. Yan and Q. J. Zhang, *Synth. Met.*, **160**, 11 (2010).
21. Y. Noskov, N. Ogurtsov, V. Bliznyuk, Y. Lvov, I. Myronyuk and A. Pud, *Appl. Nanosci.*, **12**, 1285 (2022).
22. S. Zhao, Z. Wang, J. Wang, S. Yang and S. Wang, *J. Membr. Sci.*, **376**, 83 (2011).
23. L. Xia, *Materials*, **14**, 2629 (2021).
24. M. Laridjani, J. P. Pouget, E. M. Scherr, A. G. Macdiarmid, M. E. Jozefowicz and A. J. Epstein, *Macromolecules*, **25**, 87 (1992).
25. S. Zhou, H. Zhang, Q. Zhao, X. Wang, J. Li and F. Wang, *Carbon*, **52**, 440 (2013).
26. D. Gui, C. Liu, F. Chen and J. Liu, *Appl. Surf. Sci.*, **307**, 172 (2014).
27. Y. Li, X. Zhao, Q. Xu, Q. Zhang and D. Chen, *Electrochim. Acta*, **27**, 6458 (2011).
28. X. S. Du, M. Xiao and Y. Z. Meng, *J. Polym. Sci. Part B*, **42**, 1972 (2010).
29. N. Wang, K. Cheng, H. Wu and F. Wang, *Chin. J. Mater. Res.*, **27**, 432 (2013).
30. S. Jafarzadeh, P. M. Claesson, P. E. Sundell, J. Pan and E. Thormann, *ACS Appl. Mater.*, **6**, 19168 (2014).
31. S. J. Pa Ul, B. K. Gupta and P. Chandra, *Polym. Bull.*, **1**, 17 (2020).
32. G. D. Khuspe, M. A. Chougule, S. T. Navale, S. A. Pawar and V. B. Patil, *Ceram. Int.*, **40**, 3 (2014).
33. T. Abdiryim, Z. X. Gang and R. Jamal, *Mater. Chem. Phys.*, **90**, 367 (2005).
34. Q. Feng, H. Zhang, Y. Shi, X. Yu and G. Lan, *Polymers*, **13**, 1360 (2021).
35. M. Abutalib and A. Rajeh, *J. Mater. Sci.*, **31**, 9430 (2020).
36. M. O. Ansari, M. M. Khan, S. A. Ansari, I. Amal, J. Lee and M. H. Cho, *Mater. Lett.*, **114**, 159 (2014).
37. S. D. Liu, Y. K. Ren, Z. Zhou, W. C. Chen, Z. Q. Li, F. L. Guo, L. E. Mo, J. H. Wu, L. H. Hu and S. Y. Dai, *J. Power Sources*, **329**, 225 (2016).